Journal of Applied Physics

Strong negative electrothermal feedback in thermal kinetic inductance detectors

Cite as: J. Appl. Phys. **130**, 124503 (2021); https://doi.org/10.1063/5.0064723
Submitted: 26 July 2021 • Accepted: 14 September 2021 • Published Online: 28 September 2021

Shubh Agrawal, Bryan Steinbach, James J. Bock, et al.

AIP Publishing

Journal of Applied Physics ARTICLE scitation.org/journal/jap

Strong negative electrothermal feedback in thermal kinetic inductance detectors

Cite as: J. Appl. Phys. **130**, 124503 (2021); doi: 10.1063/5.0064723
Submitted: 26 July 2021 · Accepted: 14 September 2021 ·
Published Online: 28 September 2021

Shubh Agrawal,[1,a)] Bryan Steinbach,[1,b)] James J. Bock,[1,2] Clifford Frez,[2] Lorenzo Minutolo,[1] Hien Nguyen,[2] Roger O'Brient,[2] Anthony Turner,[2] and Albert Wandui[1]

AFFILIATIONS

[1]Department of Physics, California Institute of Technology, Pasadena, California 91125, USA
[2]Jet Propulsion Lab, Pasadena, California 91109, USA

[a)]**Author to whom correspondence should be addressed:** shubh@caltech.edu
[b)]**Electronic mail:** bsteinba@caltech.edu

ABSTRACT

We demonstrate strong negative electrothermal feedback accelerating and linearizing the response of a thermal kinetic inductance detector (TKID). TKIDs are a proposed highly multiplexable replacement to transition-edge sensors and measure power through the temperature-dependent resonant frequency of a superconducting microresonator bolometer. At high readout probe power and probe frequency detuned from the TKID resonant frequency, we observe electrothermal feedback loop gain up to $\mathcal{L} \approx 16$ through measuring the reduction of settling time. We also show that the detector response has no detectable non-linearity over a 38% range of incident power and that the noise-equivalent power is below the design photon noise.

I. INTRODUCTION AND MOTIVATION

We present observations of strong negative electrothermal feedback in a thermal kinetic inductance detector (TKID). TKIDs are cryogenic bolometers that detect minute power fluctuations by measuring the temperature fluctuations of a suspended absorber.[1–6] The suspended absorber is connected to a thermal bath with a weak thermal link so that the incident power and the suspended absorber temperature are related approximately linearly. In a TKID, the temperature rise is measured through the temperature dependence of the kinetic inductance effect in a superconducting inductor on the suspended absorber. The inductor is coupled to a capacitor to form a superconducting microresonator such that the incident power is measured by the change in the resonant frequency. The resonant frequency is measured through the phase shift of a readout probe signal, which normally is at a low enough power (much less than the incident power which is being measured) such that the TKID dynamics are not altered by the probe.

Negative electrothermal feedback occurs in bolometers when the power dissipated in the temperature sensor has a negative temperature dependence. Strong electrothermal feedback through Joule heating reduces non-linearities and resolution limitations in voltage-biased transition-edge sensors[7] and reduces Johnson noise in bolometers using resistive sensors.[8] In a detector with negative electrothermal feedback, dissipated readout power decreases rapidly with increasing temperature such that temperature deviations from the operating point return to the mean more rapidly. Total power flux is held nearly constant, as readout power compensates for changes in incident power, which increases the linearity of the bolometer. In the strong electrothermal feedback regime with transition-edge bolometers, this effect reduces the time constant of the detector by an order of magnitude.[9] These benefits have led to numerous applications for transition-edge sensors, where strong electrothermal feedback produces fast, linear, and photon noise limited sensors for millimeter-wave detection[10–12] and x-ray calorimeters with eV energy resolution.[13]

Lindeman[14] proposed a mechanism through which electrothermal feedback would occur in a TKID when the frequency of the readout probe signal was detuned from the resonant frequency. Detuning the probe frequency above the TKID's resonant frequency, an increase in temperature of the suspended absorber decreases the resonant frequency due to an increase in kinetic inductance, moving the resonant frequency further from the probe

frequency. This decreases the electrical power dissipated by the probe in the resonator, which in turn decreases the temperature of the suspended absorber, resulting in negative electrothermal feedback. The feedback can be strong in resonators with high quality factors, as there is a large change in absorption of power from the probe signal for a small change in resonant frequency. We demonstrate that this feedback occurs in a TKID device of the design previously presented and characterized at low readout power in Wandui *et al.*[15] and shown in Fig. 1.

A. Modeling

We model the response of a TKID to probe signals of high power following the schematic in Fig. 2. Probe power P_{probe} enters port 1 of the transmission line and is modulated by the resonant circuit, and some phase-shifted fraction of it exits at port 2. Strong electrothermal feedback manifests as a non-linear response to high probe powers reminiscent of the Duffing oscillator. Similar behavior is observed in traditional hot quasiparticle kinetic inductance detectors due to the non-linearity of kinetic inductance.[16] To determine the non-linear behavior of a TKID, we first solve for the stable non-linear operating temperatures of the suspended absorber and then calculate the strength of the electrothermal feedback from the relation between probe power dissipation and absorber temperature.

Incident power P_{opt} plus the readout probe power dissipated in the resonator P_{abs} heat the suspended absorber. P_{abs} is a fraction of the probe power P_{probe},

$$P_{abs} = \frac{1}{2}\chi_c\chi_g P_{probe}. \tag{1}$$

The dissipated probe power is limited by the coupling efficiency χ_c of the resonator to the transmission line and the detuning efficiency χ_g of the resonator to the probe frequency. We generalize χ_c to complex coupling quality factors Q_c with complex angle ϕ_c for asymmetric resonances,[17] where $x = (f - f_r)/f_r$ is the fractional frequency detuning and Q_i and Q_r are the internal and total quality factors,

$$\chi_c = \frac{4|Q_c|Q_i}{(|Q_c| + Q_i\cos(\phi_c)^2)}, \quad \chi_g = \frac{1}{1 + 4Q_r^2x^2}. \tag{2}$$

The fractional energy loss per radian from the resonator Q_r^{-1} is a reciprocal sum of the absorption in the inductor Q_i^{-1} and loss to the transmission line $\Re\left[Q_c^{-1}\right]$,

$$Q_r^{-1} = Q_i^{-1} + \Re\left[Q_c^{-1}\right]. \tag{3}$$

At low temperatures, the resonant frequency is f_0. As the temperature rises, the frequency shifts to f_r due to the temperature dependence of the kinetic inductance effect. We assume the superconductor follows Mattis–Bardeen theory for a thin film in its frequency shift $x_{MB} = (f_r - f_0)/f_0$ and internal quality factor Q_i,

$$x_{MB} = -\frac{\gamma\alpha_k S_2 n_{qp}}{4N_0\Delta}, \tag{4}$$

$$Q_i = \frac{2N_0\Delta}{\gamma\alpha_k n_{qp} S_1}, \tag{5}$$

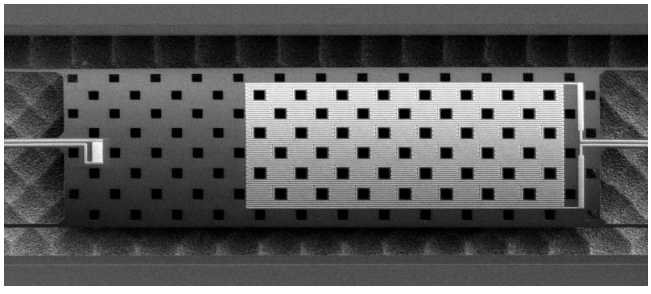

FIG. 1. SEM micrograph of the suspended absorber of a TKID of the design used for this work. The gold resistor heater is seen on the left and the meandered aluminum inductor is seen on the right. For more details on the design of the TKID, see Wandui *et al.*[15]

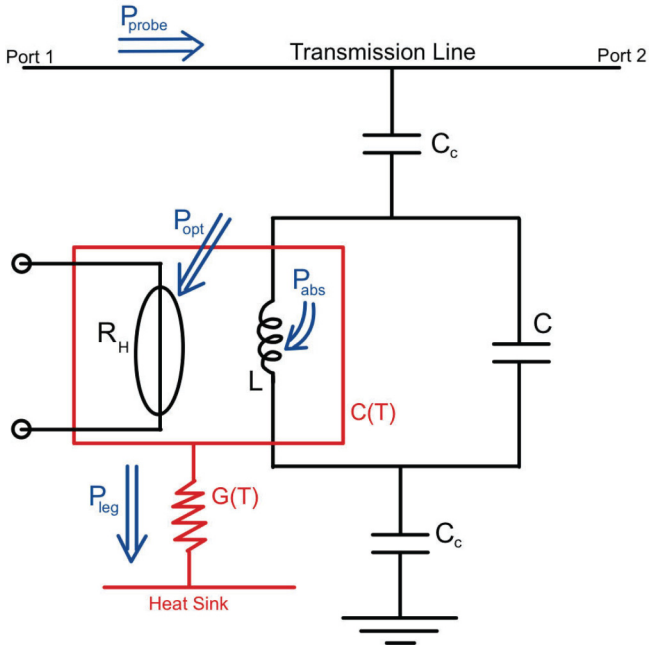

FIG. 2. Schematic and circuit diagram of the TKID. The suspended absorber, as shown in Fig. 1, is enclosed in red. The blue arrows represent the power fluxes into (P_{opt} and P_{abs}) and out of (P_{leg}) the absorber and the probe power along the transmission line (P_{probe}). Capacitors C_c weakly couple the detector to the transmission line. The inductance L and capacitance C form the TKID's superconducting microresonator.

where S_1 and S_2 are the Mattis–Bardeen derived absorption and frequency responses for a superconducting microresonator,[18] γ is the proportionality constant between perturbations in complex conductivity and surface impedance, α_k is the kinetic inductance fraction for our TKID resonator, and n_{qp} is the equilibrium quasiparticle density for a BCS superconductor at suspended absorber temperature T with gap Δ and density of states N_0. For our thin aluminum films with critical temperature T_c, we assume $\gamma = 1$, $\Delta \approx 1.76\, k_B T_c$, and $N_0 = 1.72 \times 10^{10}\, \mu\text{m}^{-3}\, \text{eV}^{-1}$. We use low temperature approximations to the Mattis–Bardeen integrals for n_{qp}, S_2, and S_1,

$$n_{qp} = 2N_0\sqrt{2\pi k_B T \Delta}\exp\left(-\frac{\Delta}{k_B T}\right), \tag{6}$$

$$S_2 = 1 + \sqrt{\frac{2\Delta}{\pi k_B T}}\exp\left(-\frac{hf}{2k_B T}\right) I_0\left[\frac{hf}{2k_B T}\right], \tag{7}$$

$$S_1 = \frac{2}{\pi}\sqrt{\frac{2\Delta}{\pi k_B T}}\sinh\left(\frac{hf}{2k_B T}\right) K_0\left[\frac{hf}{2k_B T}\right], \tag{8}$$

where I_0 and K_0 are the zeroth-order modified Bessel functions of the first and second kind, respectively.

The suspended absorber has a heat capacity $C(T)$ and is connected to a heat sink at temperature T_{bath} through a thermal conductance $G(T) = nK_c T^{n-1} = \partial P_{leg}/\partial T$. The power transferred between the suspended absorber and the heat sink is $P_{leg} = K_c(T^n - T_{\text{bath}}^n)$.

The thermal energy in the suspended absorber changes at a rate equal to net power entering and leaving the suspended absorber,

$$C(T)\frac{dT}{dt} = -P_{leg} + P_{abs} + P_{opt}. \tag{9}$$

The steady-state solutions for the temperature thus satisfy $P_{abs}(T) + P_{opt} = P_{leg}(T)$, and for stability, we additionally require $\partial P_{abs}/\partial T < \partial P_{leg}/\partial T$, as otherwise a small perturbation in temperature will grow exponentially. We show predicted stable temperature solutions for a range of probe powers in Fig. 3.

Like the Duffing oscillator, at high probe powers, the response to probe frequency sweeps splits into two stable branches. The stable branches are a cold branch with weak positive electrothermal feedback and a hot branch with strong negative electrothermal feedback. A third unstable branch exists at an intermediate temperature and experiences strong positive electrothermal feedback, so small perturbations grow rapidly away from equilibrium. We neglect this unstable solution, which is inaccessible to our experimental setup.

Qualitatively, we explain the extended hot branch and the lower bifurcation frequency in Fig. 3 as follows. If the probe frequency starts above the resonant frequency, we dissipate a small amount of power in the resonator that pushes its frequency slightly down. As we lower the probe frequency and have it approach the resonant frequency, the dissipated power grows, so the resonant frequency is further pushed down. The frequency gap must continue to close for the dissipated power to grow, so χ_g increases. Eventually, the frequency gap shrinks to zero, and the dissipated power is maximized. At this point, any further decrease in probe frequency decreases the dissipated power, and the resonant frequency begins rising and switches back to the cold branch, leaving the probe frequency well below the resonant frequency.

We term these sweeps described above, where the probe frequency is stepped down slowly in small decrements, as "downsweeps." "Upsweeps" are where we step the probe frequency up slowly in small increments, and these exhibit positive electrothermal feedback. In upsweeps, the probe frequency starts lower than the resonance frequency, and as power is dissipated in the resonator and positive electrothermal feedback becomes significant, the resonant frequency is pulled down and switches to below the probe frequency.

Non-linear kinetic inductance[16] and quasiparticle heating[19,20] could produce similar non-linearities in our devices, without producing useful electrothermal feedback that speeds up the time constant or linearizes the response. In the case of non-linear kinetic inductance, as the current in the inductor approaches the critical current, the inductance increases, and the resonant frequency decreases, mimicking electrothermal feedback from the perspective of the probe. We minimize the impact of non-linear kinetic inductance in our setup by operating the TKID at higher temperatures, where it has strong responsivity and, therefore, relatively low quality factors (≈10 000) and low current densities in the superconducting film.

Quasiparticle heating can also produce electrothermal feedback internal to the quasiparticle population but without any useful reduction in the time constant. Quasiparticle heating is reduced due to our large volume inductor, which maximizes the thermal conductance between the quasiparticles and the phonons in the superconducting film. The quasiparticle to phonon thermal

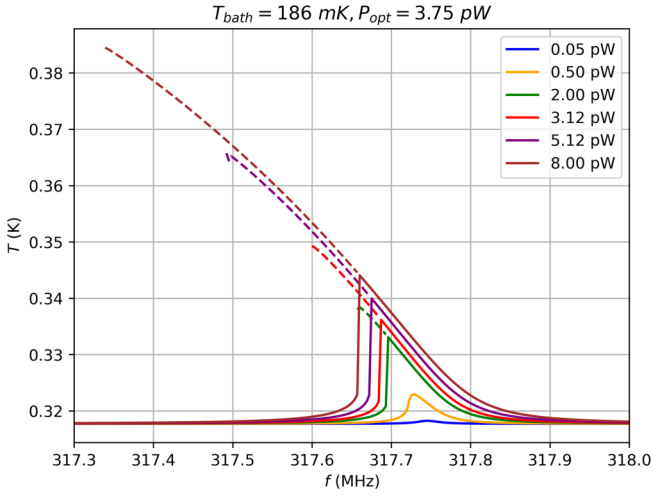

FIG. 3. Model predictions for suspended absorber temperature T under slow probe frequency sweeps. Different probe powers are shown in different colors. Solid lines indicate the cold branch, which is accessed through frequency upsweeps; dashed segments show the hot branch which is accessed through frequency downsweeps. Model parameters used are those for the device tested in Sec. II A.

conductance also benefits from high temperatures, where the quasiparticle density is high and the quasiparticle lifetime is short.

B. Loop gain and time constant

The dynamics of small perturbations in temperature can be analyzed by linearizing Eq. (9). Consider a small deviation δT from the steady-state temperature T^0 such that $T(t) = T^0 + \delta T$. We Taylor expand $P_{leg} = P^0_{leg} + G\delta T$ where $G = \partial P_{leg}/\partial T$, $P_{abs} = P^0_{abs} - G_{ETF}\delta T$, where $G_{ETF} = -\partial P_{abs}/\partial T$. With these substitutions, the linearized version of Eq. (9) becomes

$$C\frac{d\delta T}{dt} = -(G + G_{ETF})\delta T + P_{opt}. \tag{10}$$

Following the convention for transition-edge sensors,[9] we define loop gain as $\mathcal{L} = G_{ETF}/G$. Loop gain measures how strongly electrothermal feedback forces the temperature of the bolometer back to equilibrium, relative to the forcing due to the thermal link. Negative electrothermal feedback corresponds to positive loop gain due to the minus sign in the definition of G_{ETF}. Solving Eq. (10) for a step-change in P_{opt} leads to the time constant for the bolometer

$$\tau_{ETF} = \frac{1}{\mathcal{L}+1}\frac{C}{G} = \frac{1}{\mathcal{L}+1}\tau_0, \tag{11}$$

where $\tau_0 = C/G$ is the intrinsic bolometer thermal time constant.

The effective electrothermal feedback G_{ETF} is the derivative of P_{abs} with temperature, which from Eq. (1) is

$$G_{ETF} = P'_{abs}(T) = \frac{1}{2}(\chi'_c(T)\chi_g(T) + \chi_c(T)\chi'_g(T))P_{probe}. \tag{12}$$

To estimate loop gain in the strong negative electrothermal feedback regime, the term $\chi'_c(T)$ can be neglected, because it is temperature-dependent only through the internal quality factor, while $\chi'_g(T)$ is temperature-dependent through resonator frequency shifts. At the low probe frequencies of interest for TKIDs, the frequency shift effects are more significant than quality factor shifts by typically about an order of magnitude. We additionally assume that $Q'_r(T)$ is zero in $\chi'_g(T)$. Then, the temperature dependence of G_{ETF} is contained in

$$\chi'_g(T) = -8Q_r^2\chi_g(T)^2x(T)x'(T). \tag{13}$$

The fractional frequency offset between probe and resonator that maximizes $\chi'_g(T)$ is

$$\hat{x} = \frac{1}{Q_r\sqrt{12}}. \tag{14}$$

At this detuning, where the probe is between one-quarter and one-third of a linewidth above the resonant frequency, the power absorbed is

$$\hat{P}_{abs} = \frac{3}{8}\chi_c P_{probe}. \tag{15}$$

The loop gain at optimal detuning $\hat{\mathcal{L}}$ can be expressed in terms of $\beta = S_2/S_1$, $\kappa = \partial \log n_{qp}/\partial \log T$. We additionally define $\alpha = \sqrt{3}\beta\kappa/4$, in order to put the expression of the loop gain of a TKID into the same form as the loop gain of a transition-edge sensor,[9]

$$\hat{\mathcal{L}} = \frac{\alpha P_{abs}}{GT}. \tag{16}$$

C. Noise model

The intrinsic noise of a TKID contains contributions from three sources: thermal fluctuations in the suspended absorber due to the exchange of phonons in the weak thermal link, quasiparticle number density fluctuations in the superconductor due to thermal generation and recombination of quasiparticles, and readout noise from the low noise amplifier. When the TKID is operated in the strong electrothermal feedback regime, we expect a significant change in the phonon noise and small changes in generation recombination noise and readout noise. We expect our devices to be strongly phonon noise limited. The phonon noise contribution to the noise-equivalent power of the detector,

$$NEP_{\text{phonon}} = \sqrt{4k_B T^2 G\gamma_{neq}}, \tag{17}$$

includes $\gamma_{neq} \approx 0.5$, a factor that accounts for the lower temperature of the thermal bath.[8] Phonon noise will generally increase due to an increase in the total thermal power in the legs. A typical operating condition for transition-edge sensors is setting dissipated readout power equal to the incident power; for this setup, the phonon noise increases by a factor of $\sqrt{2}$ if the detector thermal conductance G is re-optimized to fix the suspended absorber temperature.

Changes in the quasiparticle generation recombination noise should be limited by the large volume of our inductor, as the quasiparticle population is in thermal equilibrium with the phonons in the suspended absorber. The readout noise should not vary much, because the decrease in coupling efficiency from detuning is compensated for by the increase in readout power, such that the absolute responsivity $P_{probe} \times dS_{21}/dP_{opt}$ is only weakly dependent on probe power in the strong electrothermal feedback regime.

We also expect an additional source of frequency-dependent noise due to finite thermal conductance within the suspended absorber and distributed heat capacity. This effect is observed in transition-edge sensors at high loop gains,[21] manifesting as a rise in noise beyond the intrinsic thermal bandwidth of the suspended absorber. Our suspended absorber is approximately 300 nm thick, much thinner than the 1000 nm thick absorbers where we have observed this effect in transition-edge sensors.[22] This reduces the thermal conductance within the absorber, which is limited by the

cross-sectional area of the suspended absorber, due to the phonon analog of the Stefan–Boltzmann law.

In addition to these intrinsic noise sources, two-level system (TLS) noise plays an important role in the noise budget of superconducting microresonators[18] but was expected to be negligible and not detected in the TKIDs studied here due to their high responsivity dx/dP_{opt}[15] at low probe powers. Due to the suppression of responsivity from electrothermal feedback, TLS noise could be enhanced and contribute significantly to TKID noise at high readout probe power and would have a magnitude proportional to $(1+\mathcal{L})S_{TLS}$, where S_{TLS} is the fractional frequency noise power spectrum due to TLS. However, due to our lack of knowledge of S_{TLS} for the TKID devices under study in this work, we are unable to make quantitative estimates of the contribution of TLS noise to the total NEP.

II. RESULTS AND DISCUSSION

We studied a single TKID at high readout probe powers using the cryostat described in Wandui *et al.*[15] and the software-defined radio system described in Minutolo *et al.*[23] To deposit incident power P_{opt} that is free of photon noise, we supplied DC to the gold heater resistor visible in Fig. 1 on the suspended absorber. The nominal incident power used in our experiments is $P_{opt} = 3.75\,\text{pW}$, which brings the aluminum inductor to a temperature $T \approx 0.33\,\text{K}$, where it has useful responsivity. At this operating temperature and bath temperature $T_{bath} = 186\,\text{mK}$, the thermal conductance is $G = K_c\,(T^n - T_{bath}^n) = 4.3 \pm 0.2\,\text{pW}$, with K_c and n determined in Sec. II A. The deposited aluminum layer of the inductor is 50 nm thick.

A. TKID characterization

To characterize the TKID resonator at low readout probe power, we obtained transmission S_{21} measurements by biasing the detector at a fixed probe power $P_{probe} = 0.1\,\text{pW}$ and sweeping the probe frequency f over 2001 equally spaced points between 312.5 and 319 MHz. We repeated this for 10 different values of bath temperature T_{bath} between 114 and 439 mK. A least squares fit of the S_{21} curves to Eq. (18) gives us the resonant frequency f_r dependent on T_{bath}, which when fitted using Eqs. (4), (6), and (7), estimates $|Q_c| \approx 13\,500$, $\phi_c \approx 0.3$, $T_c = 1.32 \pm 0.01\,\text{K}$, and $\alpha_k = 0.50 \pm 0.03$.

With the resonator now calibrated as a thermometer, we characterize the weak thermal link by sweeping the incident power P_{opt} in 31 steps between 0 and 23.4 pW with $T_{bath} = 186\,\text{mK}$. Least squares fits to the responses determine the dependence of f_r on P_{opt}. The approximation $P_{opt} \approx P_{leg}$ in Eqs. (9) and (1) gave us $f_0 = 317.889 \pm 0.005\,\text{MHz}$, $K_c = 185 \pm 3\,\text{pW/K}^n$, and $n = 3.23 \pm 0.02$. Our value of $n \approx 3$ is consistent with similar bolometers with thin silicon nitride support legs used in BICEP/Keck.[15]

B. Non-linear S_{21} curves

We measured non-linear S_{21} by biasing the detector at a range of fixed probe powers P_{probe} and performing both up- and downsweeps, over 3000 equally spaced probe frequencies f between 316 and 318.4 MHz. The bath temperature was regulated to 186 mK, and we fixed the incident power at $P_{opt} = 3.75\,\text{pW}$. The predicted S_{21} is given by

$$S_{21}(f) = 1 - \frac{Q_r}{Q_c}\frac{1}{1 + j2Q_r x}, \tag{18}$$

where Q_r and x are determined by solving for the stable suspended absorber temperature as described in Sec. I A.

Figure 4 shows the measured and predicted S_{21} frequency sweeps when probe power at the chip is 0.5, 5, and 8 pW.

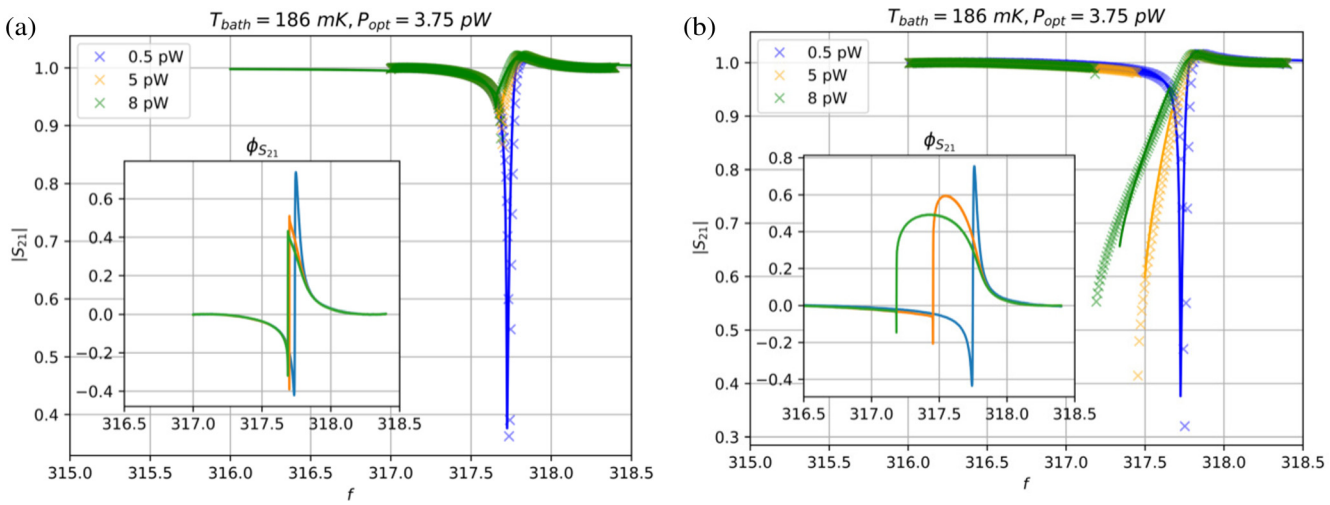

FIG. 4. Crosses show the measured S_{21} magnitude plotted against frequency for (a) upsweeps (frequency is stepped up in gradual increments) and (b) downsweeps (frequency is stepped down in gradual decrements). Model predictions are given by lines. Insets show measured S_{21} phase. Strong hysteresis is seen for downsweeps at probe powers of the order of a few pW, when P_{probe} is comparable to P_{opt}.

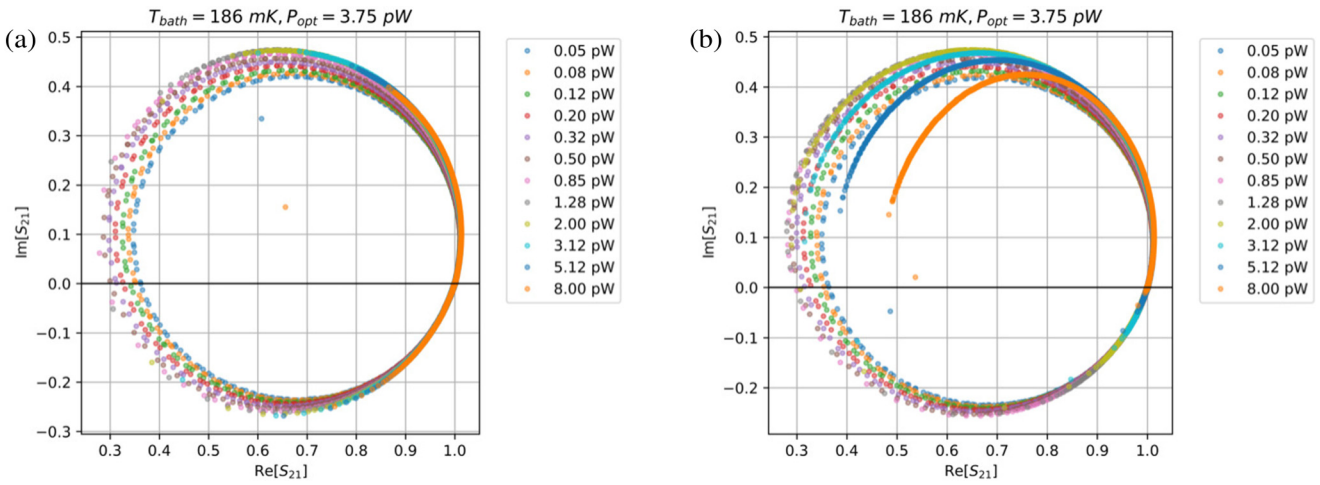

FIG. 5. S_{21} measured at various probe powers plotted in *Re-Im* space for (a) upsweeps (frequency is stepped up in gradual increments) and (b) downsweeps (frequency is stepped down in gradual decrements). Strong non-linearity is seen for downsweeps when P_{probe} is comparable to P_{opt} in the form of deviations from an exact circle.

Directional hysteresis is absent at 0.5 pW but shows up strongly at 5 and 8 pW. For frequency downsweeps at the higher probe powers, the resonance frequency is pushed down as predicted by the negative electrothermal feedback model. At the highest probe power setting with $P_{probe} = 8$ pW, we observed that the lower bifurcation frequency of the hysteresis branch deviates by a few MHz from the resonance frequency obtained at low probe power.

Figure 5 shows measured S_{21} frequency sweeps in the *Re-Im* space, at 12 different values of P_{probe} between 0.05 pW and 8.00 pW. S_{21} traces a circle in the complex plane for linear detectors. We observe that this non-linear deviation increases with probe powers and the deviation is higher for downsweeps than for upsweeps.

These non-linear S_{21} frequency downsweeps demonstrate that the detector can be biased into the hot branch (with significant negative electrothermal feedback) by applying a high P_{probe} at a frequency higher than resonance and then sweeping the frequency down to operating frequency in gradual decrements. The gold resistor heater on our test device allows for another method for biasing into the hot branch, as described in Sec. II C.

C. Speed of response

We measured bolometer time constants on the hot branch at probe powers ranging from 0.05 to 8 pW. We applied probe signals at frequencies f between 317.0 and 318.0 MHz spaced by 50 kHz to the detector with bath temperature regulated to $T_{bath} = 186$ mK. The incident power pulses with a 34 pW square impulse several time constants wide (0.05 s) to bias the detector into the hot branch. After the pulse, the incident power oscillates in a 1.92 Hz square wave between 3.65 and 3.85 pW. We recorded S_{21} for 5 s intervals at a sample rate of 20 kHz. Stacked S_{21} traces at low and high negative electrothermal feedback are shown in Fig. 6. Fitting the exponential decay of detector response S_{21} at the edge of the applied square wave estimates the time constant τ. This gives us the loop gain $\mathcal{L}$ by Eq. (11).

We show the observed loop gain as a function of probe frequency and power, along with our model predictions, in Fig. 7. The highest value $\mathcal{L} = 15.7 \pm 1.3$ observed was at $P_{probe} = 8$ pW and $f = 317.45$ MHz. Our model slightly underestimates the speed-up

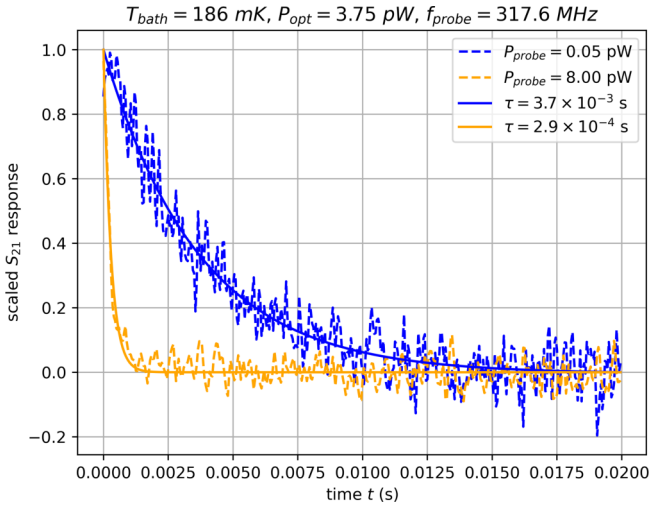

FIG. 6. Measured S_{21} step responses to a small change in incident power at low (blue) and high (orange) probe power, averaged over ≈10 periods shown in dotted lines. Solid lines show the fit to the exponential decay at this edge of the applied P_{opt} square wave. For clarity, the data are scaled and shifted along the y axis, such that the response range for both is (0, 1]. At high probe power, the time for S_{21} to reach a steady state is reduced dramatically due to strong negative electrothermal feedback.

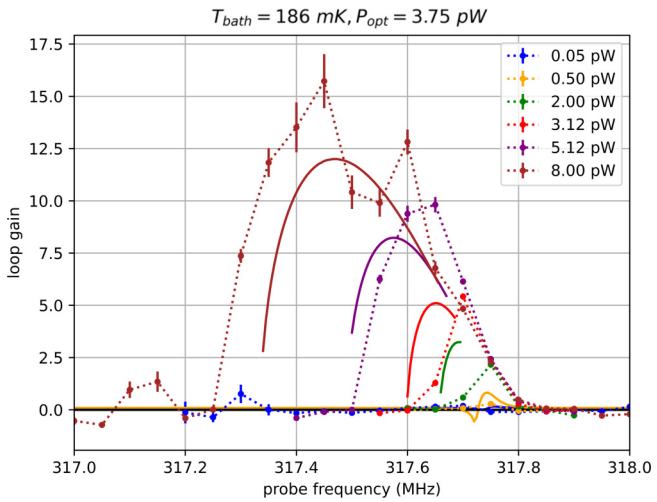

FIG. 7. Measured loop gains plotted against probe frequency (in MHz) at incident power $P_{opt} = 3.75\,\text{pW}$ and a range of probe powers P_{probe}. Measured data points are connected by dotted lines; solid lines give model predictions between the two bifurcation frequencies. Higher values of $\mathcal{L}$ are obtained at higher probe powers in good agreement with predictions.

of the bolometer time constant, which will be investigated in future work. We did not observe the detector jumping from its steady state in the hot branch back to the cold branch, without changes in probe signal or removing the optical power.

D. Linearity of response

To measure linearity in the strong negative electrothermal feedback regime, we biased the TKID with $P_{probe} = 5.12\,\text{pW}$, $f = 317.65\,\text{MHz}$ while regulating the bath temperature to $T_{bath} = 186\,\text{mK}$, where loop gain was previously measured to be $\mathcal{L} \approx 10$ at $P_{opt} = 3.75\,\text{pW}$. We swept incident power P_{opt} over a wide range, from which we select a region from 3.5 to 4.9 pW (or 8% below and 30% above the nominal 3.75 pW) where the response is highly linear. The top panel of Fig. 8 shows the detector response to the incident power sweep in S_{21} phase. We fitted this response to a linear model, as shown in the two panels of Fig. 8. The residuals (lower panel) are dominated by measurement noise and indicate linearity better than 0.1% in this operational range.

E. NEP measurements

We measured the noise-equivalent power (NEP) of the TKID over a range of probe frequencies and powers. As in the time constant measurements, we biased the detector into the hot branch by pulsing the incident power after applying the probe signal. We rotate the S_{21} timestream so that the response to a small optical power step is in the real direction. Next, we convert the S_{21} timestream from ADC units to power units by scaling by the responsivity measured by the square wave during the time constant measurement at the same optical power, probe power, and probe frequency. The NEP amplitude spectrum is shown in Fig. 9 for

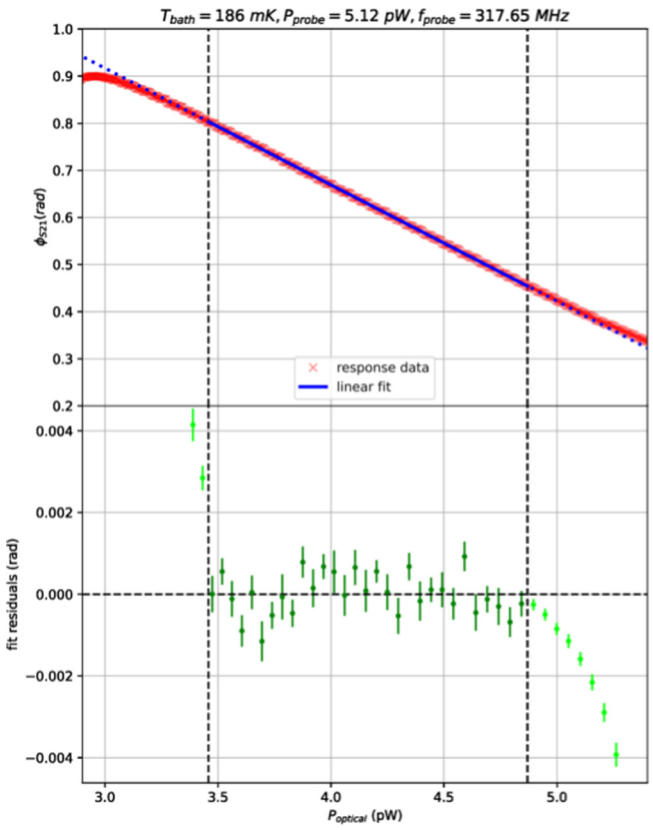

FIG. 8. Above, the response of the detector in S_{21} phase over a range of incident power in red, along with a linear fit in blue. Below, the binned residual difference between data and linear fit, giving a reduced $\chi^2 \approx 2$. The two vertical black dotted lines delimit the selected highly linear region; the extrapolation to the linear fit is the dotted blue line outside the region.

$P_{probe} = 5.12\,\text{pW}$ and $f = 317.65\,\text{MHz}$ for both the real noise, which includes detector noise and readout noise, and the imaginary noise, which traces the readout noise level and cannot be used to detect optical power. The real noise rises at kHz frequencies, suggestive of internal thermal resistance and decoupled heat capacities as discussed in Sec. I C.

We suspect common-mode environmental noise, likely from thermal fluctuations or RF-interference susceptibility that are detector–detector correlated, to be responsible for the higher noise amplitude between 10 and 30 Hz and the $1/f$ knee at $\approx$10 Hz.[15] Because we recorded noise for only a single detector, we did not implement common-mode noise removal to obtain the results shown in Fig. 9. Common-mode noise removal, such as pair differencing or principal components analysis, has been previously proven effective when reading out a small array of multiple detectors, achieving phonon-limited NEPs with a $1/f$ knee at $\approx$0.1 Hz for the same detector design.[15]

Figure 10 shows the NEP at all measured probe powers and frequencies. The NEP is averaged over 10–30 Hz to minimize the

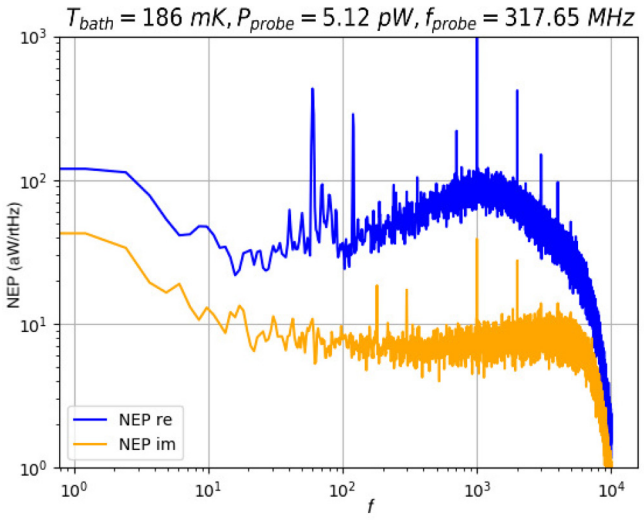

FIG. 9. Noise-equivalent power (NEP) amplitude spectrum for $P_{probe} = 5.12$ pW, $f = 317.65$ MHz, and $P_{opt} = 3.75$ pW on the hot branch. The blue curve shows detector noise and readout noise in the direction in the complex plane that changing incident power changes S_{21}, while the yellow curve traces the readout noise floor in the quadrature direction, which is insensitive to changes in optical power.

impact of the excess low-frequency noise and the rise in kHz high-frequency noise. There is a probe frequency at all probe powers that achieves a NEP of 25 aW/rtHz. This is below the intended photon noise of 38 aW/rtHz but well above the expected phonon noise of 14 aW/rtHz. We believe that the NEP is limited by environmental noise, as we have observed phonon-limited noise with much lower $1/f$ knees in a TKID of the same design.[15]

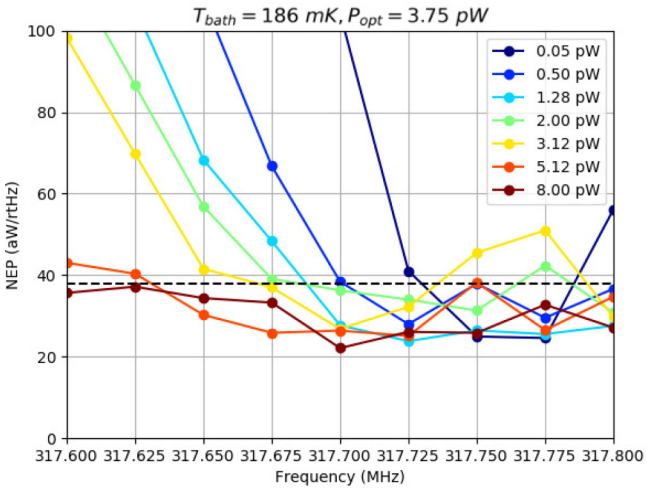

FIG. 10. NEP at several probe fixed signals P_{probe} and f on the negative electrothermal feedback hot branch.

III. CONCLUSION

We have demonstrated negative electrothermal feedback in a TKID biased at readout probe powers comparable to the design incident power through the speed-up in bolometer response time. The maximum speed-up we observed was a factor of $\tau_0/\tau = 1 + \mathcal{L} = 16.7 \pm 1.3$ at $P_{probe} = 8$ pW and $P_{opt} = 3.75$ pW. Equation (16) indicates that we can attain higher values of loop gain by increasing β, which could be achieved by designing a device with a higher film critical temperature T_c or by reducing the operating probe frequency.

At a bias of $P_{probe} = 5.12$ pW, we observed a highly linear response in phase $\phi_{S_{21}}$ for $P_{opt} = 3.5$–4.9 pW. We also provide noise-equivalent power (NEP) measurements of the detector, which demonstrate that the noise performance remains comparable to nominal TKID values when they are biased at low probe powers. Our NEP measurements do not reach the phonon noise floor, so we cannot yet rule out whether operating at a high probe power introduces additional noise at the 15 aW/rtHz level.

In this work, we operated only a single detector in the negative electrothermal feedback regime. As the TKID is intended to be a multiplexable detector, it remains to be seen what the practical implication of high probe power operation is on multiplexing. We anticipate an increase in the dynamic range requirement of the readout due to the decrease in responsivity relative to the probe power. Additionally, moving resonators with probe power can impact resonator collisions.

We see hints of the internal thermal structure to the detector in our NEP measurements, manifesting as a characteristic rise at high frequency. We intend to measure the incident power to S_{21} transfer function in the frequency domain to clarify the internal thermal structure of the TKID. The results presented here indicate that operating the detector with high electrothermal feedback does not degrade the noise in single devices; we leave further noise performance tests using common-mode noise removal to future work.

The increase in speed due to negative electrothermal feedback could allow TKIDs to be practical in low incident power applications such as in narrow bandwidth line intensity mapping spectrometers, where low thermal conductance would lead to the TKID being otherwise too slow. The increase in speed could also be useful in calorimeters, where energy resolution is inversely proportional to the square root of the loop gain.[9]

ACKNOWLEDGMENTS

Our work was carried out at the Jet Propulsion Laboratory, Caltech, under contract from the National Aeronautics and Space Administration. We thank Mark Lindeman and Jonas Zmuidzinas for insightful discussion. Shubh Agrawal's work was supported by the Dr. Gary Stupian SURF Fellowship.

DATA AVAILABILITY

The data that support the findings of this study are available from the corresponding author upon reasonable request.

REFERENCES

[1]G. Ulbricht, B. A. Mazin, P. Szypryt, A. B. Walter, C. Bockstiegel, and B. Bumble, Appl. Phys. Lett. **106**, 251103 (2015).
[2]O. Quaranta, T. Cecil, L. Gades, B. Mazin, and A. Miceli, Supercond. Sci. Technol. **26**, 105021 (2013), arXiv:1304.3387.
[3]M. Arndt, S. Wuensch, C. Groetsch, M. Merker, G. Zieger, K. Peiselt, S. Anders, H.-G. Meyer, and M. Siegel, IEEE Trans. Appl. Supercond. **27**, 1 (2017).
[4]A. V. Timofeev, V. Vesterinen, P. Helistö, L. Grönberg, J. Hassel, and A. Luukanen, Supercond. Sci. Technol. **27**, 025002 (2014).
[5]S. O. Dabironezare, J. Hassel, E. Gandini, L. Grönberg, H. Sipola, V. I. Vesterinen, and N. Llombart, IEEE Trans. Terahertz Sci. Technol. **8**, 746–756 (2018).
[6]R. A. Wernis, "Characterizing a resonator bolometer array," Senior thesis (Major) (California Institute of Technology, 2013).
[7]K. D. Irwin, Appl. Phys. Lett. **66**, 1998 (1995).
[8]J. C. Mather, Appl. Opt. **21**, 1125 (1982).
[9]K. D. Irwin and G. C. Hilton, Cryogen. Particle Detect. **99**, 63 (2005), ISBN: 9783540201137.
[10]A. J. Anderson, P. A. R. Ade, Z. Ahmed, J. S. Avva, P. S. Barry, R. B. Thakur, A. N. Bender, B. A. Benson, L. Bryant, K. Byrum, J. E. Carlstrom, F. W. Carter, T. W. Cecil, C. L. Chang, H.-M. Cho, J. F. Cliche, A. Cukierman, T. de Haan, E. V. Denison, J. Ding, M. A. Dobbs, D. Dutcher, W. Everett, K. R. Ferguson, A. Foster, J. Fu, J. Gallicchio, A. E. Gambrel, R. W. Gardner, A. Gilbert, J. C. Groh, S. T. Guns, R. Guyser, N. W. Halverson, A. H. Harke-Hosemann, N. L. Harrington, J. W. Henning, G. C. Hilton, W. L. Holzapfel, D. Howe, N. Huang, K. D. Irwin, O. B. Jeong, M. Jonas, A. Jones, T. S. Khaire, A. M. Kofman, M. Korman, D. L. Kubik, S. Kuhlmann, C.-L. Kuo, A. T. Lee, E. M. Leitch, A. E. Lowitz, S. S. Meyer, D. Michalik, J. Montgomery, A. Nadolski, T. Natoli, H. Nguyen, G. I. Noble, V. Novosad, S. Padin, Z. Pan, P. Paschos, J. Pearson, C. M. Posada, W. Quan, A. Rahlin, D. Riebel, J. E. Ruhl, J. T. Sayre, E. Shirokoff, G. Smecher, J. A. Sobrin, A. A. Stark, J. Stephen, K. T. Story, A. Suzuki, K. L. Thompson, C. Tucker, L. R. Vale, K. Vanderlinde, J. D. Vieira, G. Wang, N. Whitehorn, V. Yefremenko, K. W. Yoon, and M. R. Young, J. Low Temp. Phys. **199**, 320 (2020).
[11]C. Zhang, P. A. R. Ade, Z. Ahmed, M. Amiri, D. Barkats, R. B. Thakur, C. A. Bischoff, J. J. Bock, H. Boenish, E. Bullock, V. Buza, J. Cheshire, J. Connors, J. Cornelison, M. Crumrine, A. Cukierman, M. Dierickx, L. Duband, S. Fatigoni, J. P. Filippini, G. Hall, M. Halpern, S. Harrison, S. Henderson, S. R. Hildebrandt, G. C. Hilton, H. Hui, K. D. Irwin, J. Kang, K. S. Karkare, E. Karpel, S. Kefeli, J. M. Kovac, C. L. Kuo, K. Lau, K. G. Megerian, L. Moncelsi, T. Namikawa, H. T. Nguyen, R. O'Brient, S. Palladino, N. Precup, T. Prouvé, C. Pryke, B. Racine, C. D. Reintsema, S. Richter, A. Schillaci, B. Schmitt, R. Schwarz, C. D. Sheehy, A. Soliman, T. S. Germaine, B. Steinbach, R. V. Sudiwala, K. L. Thompson, C. Tucker, A. D. Turner, C. Umiltà, A. G. Vieregg, A. Wandui, A. C. Weber, D. V. Wiebe, J. Willmert, W. L. K. Wu, E. Yang, K. W. Yoon, E. Young, and C. Yu, J. Low Temp. Phys. **199**, 968 (2020).
[12]B. J. Koopman, N. F. Cothard, S. K. Choi, K. T. Crowley, S. M. Duff, S. W. Henderson, S. P. Ho, J. Hubmayr, P. A. Gallardo, F. Nati, M. D. Niemack, S. M. Simon, S. T. Staggs, J. R. Stevens, E. M. Vavagiakis, and E. J. Wollack, J. Low Temp. Phys. **193**, 1103 (2018).
[13]P. Szypryt, G. C. O'Neil, E. Takacs, J. N. Tan, S. W. Buechele, A. S. Naing, D. A. Bennett, W. B. Doriese, M. Durkin, J. W. Fowler, J. D. Gard, G. C. Hilton, K. M. Morgan, C. D. Reintsema, D. R. Schmidt, D. S. Swetz, J. N. Ullom, and Y. Ralchenko, Rev. Sci. Instrum. **90**, 123107 (2019).
[14]M. A. Lindeman, J. Appl. Phys. **116**, 024506 (2014).
[15]A. Wandui, J. Bock, C. Frez, M. Hollister, L. Minutolo, H. Nguyen, B. Steinbach, A. Turner, J. Zmuidzinas, and R. O'Brient, J. Appl. Phys. **128**, 044508 (2020), see arXiv:2001.08887.
[16]L. J. Swenson, P. K. Day, B. H. Eom, H. G. Leduc, N. Llombart, C. M. McKenney, O. Noroozian, and J. Zmuidzinas, J. Appl. Phys. **113**, 104501 (2013).
[17]M. S. Khalil, M. J. A. Stoutimore, F. C. Wellstood, and K. D. Osborn, J. Appl. Phys. **111**, 054510 (2012).
[18]J. Zmuidzinas, Annu. Rev. Condens. Matter Phys. **3**, 169 (2012).
[19]C. N. Thomas, S. Withington, and D. J. Goldie, Supercond. Sci. Technol. **28**, 045012 (2015).
[20]T. Guruswamy, C. N. Thomas, S. Withington, and D. J. Goldie, Supercond. Sci. Technol. **30**, 064006 (2017).
[21]S.-F. Lee, J. M. Gildemeister, W. Holmes, A. T. Lee, and P. L. Richards, Appl. Opt. **37**, 3391 (1998).
[22]S. Kernasovskiy, "Measuring the polarization of the cosmic microwave background with the Keck Array and BICEP2," Ph.D. thesis (Stanford University, 2020).
[23]L. Minutolo, B. Steinbach, A. Wandui, and R. O'Brient, IEEE Trans. Appl. Supercond. **29**, 1 (2019).